

The University of Maine

DigitalCommons@UMaine

Honors College

Spring 5-2024

A Study Into the Fundamentals and Enhancements of Solenoid Based Accelerators

William Poole

University of Maine - Main, william.p.poole@maine.edu

Follow this and additional works at: <https://digitalcommons.library.umaine.edu/honors>



Part of the [Power and Energy Commons](#)

Recommended Citation

Poole, William, "A Study Into the Fundamentals and Enhancements of Solenoid Based Accelerators" (2024). *Honors College*. 886.

<https://digitalcommons.library.umaine.edu/honors/886>

This Honors Thesis is brought to you for free and open access by DigitalCommons@UMaine. It has been accepted for inclusion in Honors College by an authorized administrator of DigitalCommons@UMaine. For more information, please contact um.library.technical.services@maine.edu.

A STUDY INTO THE FUNDAMENTALS AND ENHANCEMENTS OF SOLENOID
BASED ACCELERATORS

by

William Poole

A Thesis Submitted in Partial Fulfillment
of the Requirements for a Degree with Honors
(Electrical Engineering)

The Honors College

University of Maine

May 2024

Advisory Committee:

David Kotecki, Associate Professor, Advisor

Nuri Emanetoglu, Associate Professor

Donald Hummels, Professor

© 2023 Poole

All Rights Reserved

ABSTRACT

The utilization of Solenoid-Based Accelerators (SBAs) is complicated due to the multitude of interacting variables in the design of the system. Additionally, SBAs also known as coilguns, are typically inefficient and have a peak efficiency of around 22% [1]. Even with the low efficiency, there is much interest in coilgun systems due to their ability to accelerate objects faster than chemical reactions, with speeds reaching 11km/s [1,2]. In addition to the peak speed, there are other advantages such as the reduced contact with the projectile and controllable launch speeds which allow for applications including the launching of nanosatellites [2]. With SBAs there are many design aspects to manage. These include, energy supply, timing control, and force generation. Each of these categories has variables that interact with each other that affect system design and efficiency. This paper is focused on the solenoids that accelerate the payload. This is where energy conversion occurs. In addition to research into prior work on these topics, a MATLAB program was developed to examine solenoid designs. A physical coilgun was fabricated to better understand the key issues in implementing a coilgun system. Experimental results show that correlations exist between the armature, solenoid, initial conditions, power, and system parameters. Furthermore, altering the geometry of the solenoid affects single stage exit velocity. Modification of the solenoid geometry may result in a reduction in efficiency.

ACKNOWLEDGEMENTS

I would like to acknowledge the Center for Undergraduate Research for funding this project. Allowing for a test system to accompany the research allowing the theoretical data to be tested experimentally. As well as helping this process it has made the process more enjoyable and educational with the difficulties of implementation.

I would also like to thank everyone who has helped with this project, the committee as David Kotecki, Donald Hummels, and Nuri Emanetoglu, the cohorts as Austin Morin, Dyllon Dunton, and Marc Michaud. Without their insight into many problems this may have never been finished, and to that I thank them all.

PREFACE/FOREWORD

This paper was made along with a project designed for an electrical engineering capstone. If this concept is to be further tested, I would recommend a system designed exclusively for testing single-stage implementations. Additionally, a further optimized system may utilize many of the mentioned modifications, especially alterations of the armature shape. In regards to these changes the synchronous switching has sparked many ideas while writing this such as back driving the coils to make the force curve flip while the armature passes through or using two interwoven solenoids to accelerate field cancellation at the center, similar to magnetic pickup hand tools.

TABLE OF CONTENTS

INTRODUCTION	1
Electromagnetic Theory and Formulae.....	2
Estimating Equations	3
Field and Simulation Equations	5
Review of Previous Coilgun Designs	7
Induction-Type.....	7
Reluctance-Type	9
Multi-Stage	10
Energy Sources	11
Control Layouts	12
Solenoids.....	13
Axial-Shape Manipulations	16
Radial-Shape Manipulations.....	20
Radial Manipulations of Armature	20
Radial Manipulations of Coil Housing	23
MATLAB Simulations	25
Code Documentation	26
Simulation Results	27
Experimental Testing	31
System.....	31

Testing Procedure	32
Experimental Results	33
DISCUSSION.....	38
CONCLUSION.....	40
BIBLIOGRAPHY.....	41
APPENDICES	44
Appendix A: Simulator Code.....	44
Appendix B: System Documentation.....	45
Appendix C: Plotted Data	47

LIST OF FIGURES

Figure 1: Side view of an induction type coilgun [6]	8
Figure 2: Schematic of referenced induction type coilgun [6]	8
Figure 3: Side view of an reluctance type coilgun [5]	9
Figure 4: Schematic of referenced reluctance type coilgun [8]	10
Figure 5: Referenced Mutli-stage Type System Schematic [9]	11
Figure 6: Reluctance design power supply (Spot Welders) [11]	12
Figure 7: Coilgun Capacitor bank showcase [8]	12
Figure 8: Concept of synchronous switching discharging circuit [12]	13
Figure 9: Example force curve across a typical solenoid [5]	14
Figure 10: Example curve of reluctance/field across a solenoid [5]	14
Figure 11: Variation of inductance of drive coils during launch [13]	15
Figure 12: Derivative of inductance of drive coils during launch [13]	15
Figure 13: Solenoid cross section for axial manipulations [14]	16
Figure 14: Field (a) and force (b) of a solenoid as length is varied [14]	16
Figure 15: Number of turns of a fixed length wire solenoid as length increases	17
Figure 16: Force generated by a solenoid as volume fluctuates [14]	18
Figure 17: Initial State of Radially Modified System [15]	20
Figure 18: Final State of Radially Modified System [15]	21
Figure 19: Results of Geometrical Optimization of Armature	21

Figure 20: Solenoid armature and coil parameters for radial changes [16] 22

Figure 21: Force response to solenoid guider thickness (W) variation [16] 23

Figure 22: Concept of non-cylindrical drive coils for coilguns [17] 24

Figure 23: Velocity Loss at Solenoid Discharge [13] 25

Figure 24: Control solenoid cross section profile 26

Figure 25: B-field (a), gradient of B across z (B) of control solenoid 27

Figure 26: Triangular solenoid cross section profile 28

Figure 27: B-field (a), gradient of B across z (B) of triangle solenoid 28

Figure 28: Horn solenoid cross section profile 29

Figure 29: B-field (a), gradient of B across z (B) of horn solenoid 30

Figure 30: Velocity of system as a function of charge voltage 34

Figure 31: Efficiency average of system across charge voltages 34

Figure 32: Minimum, average, and maximum velocities from drive coil shapes 35

Figure 33: Efficiencies from different drive coil shapes 36

LIST OF TABLES

Table 1: Commonly Used Variables and Definitions	2-3
Table 2: Simulated data from advance discharge circuit	13
Table 3: Optimum solenoid parameters based on wire length	19
Table 4: Optimum solenoid parameters based on wire gauge	19
Table 5: Measured parameters of control solenoid	32
Table 6: Measured parameters of triangular solenoid	32-33
Table 7: Measured parameters of horn solenoid	33
Table 8: Calculated results of various solenoid shapes	37

INTRODUCTION

Solenoid Based Accelerators (SBAs), or coilguns are a type of Electro-Magnetic Launcher (EML) which are typically utilized to accelerate payloads at exceedingly high speeds, from 460m/s up to 11km/s [1,2]. There are two main types of EMLs, railguns and coilguns [2]. Railguns utilize two conducting rails to complete a circuit and the field generated by the rails accelerate the projectile, which disconnect when a projectile exits the system. Coilguns utilize electromagnetic drive solenoids to pull the projectile once activated and are deactivated by a control circuit. Coilguns are the focus of this research due to the non-contacting method of launching.

SBAs rely on solenoids to operate. The solenoids generate magnetic fields to accelerate a projectile or an armature. Proper design is important for maximum transfer of electrical and magnetic energy to kinetic energy. Typically, the method of enhancing performance is by pushing current through the system with currents ranging up to 1.72MA or 1.8MA [2]. The geometry of these coils directly relates to a solenoids ability to accelerate a projectile. With a focus on solenoid/drive coil geometry, the overarching variables can be set as: axial cross-section (S_a), radial cross section (S_r), length (L), radius (r), and conductor size. In addition, there are other parameters that can be modified such as conductor material, super cooling, system supply, or control system. The focus on the shape of these solenoids is due to the geometrical relationships between their design and their force output.

There are two main variations of the coilgun design, induction and reluctance type systems [3]. The differences between these are in the armature. Induction type designs utilize induced voltage on the armature to generate an electromagnet, which is then

accelerated by the drive coils. Reluctance type designs utilize a ferromagnetic armature which is pulled by the drive coils without the induced current. Both the inductance or reluctance type rely upon the properties of the drive coils to accelerate the projectile.

This thesis describes the main aspects of a SBA. First, the relevant theory and formulas for electromagnetic acceleration are introduced. Then for reference, available documented designs for induction and reluctance designs are reviewed. Then research on the solenoid design will be presented. Both simulated and experimental results will be discussed.

Electromagnetic Theory and Formulae

With SBA designs there are a large number of formulae utilized in the analysis of the solenoid. Table 1 lists the variables used in the design.

Variable	Definition	Unit
V	Volume	m ³
M	Mass	Kg
\vec{F}	Force	N
L	Inductance	H (Henry)
μ_0	Permeability of Free Space	H/m ($4\pi \cdot 10^{-7}$)
μ_r	Relative Permeability	unitless
χ_m	Magnetic Susceptibility ($\chi_m = \mu_r - 1$)	unitless
N	Number of turns	unitless
I	Current	A
V	Voltage	V

V_{emf} OR $V_{emf,total}$	Voltage due to magnetic Induction	V
V_L	Voltage Across Inductor	V
S_a	Axial cross-section	m^2
S_r	Radial cross-section	m^2
L	Length	m
R	Radius	m
U	Velocity	m/s
U_{exit}	Exit Velocity	m/s
Φ	Magnetic Flux	Wb (weber)
\vec{B}	Magnetic Flux Density	T or wb/m ²
\vec{H}	Magnetic Field	A/m
\vec{M}	Magnetization	A/m
F	Magnetomotive force	AT (Ampere Turn)
\mathcal{R}	Reluctance	AT/wb or H ⁻¹

Table 1. Commonly Used Variables and Definitions

Estimating Equations

Estimating equations are used as a preliminary design concept to estimate how a system would perform without an in-depth analysis. With an in-depth analysis, effects of inductance, solenoid shape, and material saturation would be accounted for. The following equations 1 and 2 showcase an estimate for exit velocity and force output of a solenoid [4].

$$[1] U_{exit} = \sqrt{\frac{2}{m} * V * \mu_0 * \chi_m * N^2 * I^2}$$

$$[2] \vec{F} = V * \chi_m * \mu_0 * H * \frac{d\vec{H}}{dx}$$

The above equations show a relationship between the final velocity of a projectile based upon its volume, mass, magnetic properties (χ_m), the number of turns in the solenoid, and the current supplied into the solenoid. Furthermore, equation 2 also incorporates a geometric relationship with change of magnetic field over a distance. However, this method of modeling is inaccurate as manipulation of the solenoid shape will affect the performance of the coilgun and the equations are based upon 100% energy transfer from the magnetic field [4]. Equation 1 assumes all energy is transferred to kinetic energy, and equation 2 does not account for magnetic saturation or field alignment [4].

In addition to the estimating equations there are many software packages made for magnetic analysis. One example for direct analysis from Sandia National Labs is their Slingshot program. There are many programs designed for simply modeling magnetic fields and their shapes, Ansys has their Maxwell program, QuickField is a fast modeling software, Finite Element Method Magnets or Femm4.2 has MATLAB integration allowing for advance utilization of MATLABs existing library of functions. These software and others such as Elmers FEM can be utilized to generate optimum shapes through repeated simulation, and the force curves can be documented with reduced programming complexity.

Field and Simulation Equations

To obtain more accurate equations two methods are discussed: the magnetic moment and the reluctance methods.

Magnetic Moment Method

To calculate the force on a projectile, two things are needed: the field experienced by the magnetic moment and the magnetic moment itself. The equations for deriving the force are given below. This will be utilized in turn to calculate the velocity based on the supplied current, drive coil path, and magnetic material of the armature as μ_r or χ_m . The calculation of velocity is iterative, utilizing the equations in their given forms below allows simple parameter inputs.

Equation (3) is the Biot-Savart Law which generates the field (\vec{H}) from an electromagnet with a shape based on a current path ($d\vec{l}$), distance to a point of interest (\hat{r}), with a supplied current (I).

$$[3] \vec{H} = \int_l \frac{I * d\vec{l} \times \hat{r}}{4\pi * (|\vec{r}|^2)}$$

Equation (4) is a relation of magnetic field intensity (\vec{H}) to magnetic flux density (\vec{B}) via magnetic permeability ($\mu_r * \mu_0$).

$$[4] \vec{H} * \mu_r * \mu_0 = \vec{B}$$

Equation (5) relates magnetization (\vec{M}) and magnetic field to magnetic flux density.

$$[5] (\vec{H} + \vec{M}) * \mu_0 = \vec{B}$$

Equation (6) relates magnetization to magnetic field with magnetic susceptibility (χ_m) and relative permeability.

$$[6] \vec{M} = \chi_m * \vec{H} = (\mu_r - 1) * \vec{H}$$

Equation (7) is the force equation for a magnetic moment, this equation is a derivative in 3 dimensions of the energy in a magnetic moment [4].

$$[7] \vec{F} = \nabla(\vec{m} \cdot \vec{B}) = \mu_0 * \nabla(\vec{m} \cdot \vec{B})$$

Reluctance Method

The alternative method to calculate the force on a magnetic core uses the reluctance (\mathcal{R}) of the magnetic core, as well as the magnetic motive force (F) received by the core. The equations for this method are given below.

Equation (8) is the formula for reluctance based upon length (l), cross section (S), and permeability of the magnetic core [5].

$$[8] \mathcal{R} = \frac{l}{\mu_0 \mu_r * S}$$

Equation (9) is the formula for magnetomotive force (F) based upon reluctance under magnetic flux (Φ) [5]. Magnetic Flux can be calculated from equations 3 and 4 and then integrating magnetic flux density over the materials cross-section.

$$[9] \vec{F} = \mathcal{R} * \Phi$$

Equation (10) showcases the energy stored in the magnet based upon induced Magnetive Motive force (MMF) [5].

$$[10] \vec{E} = \int \vec{F} d\Phi$$

Equation (11) is the reluctance version of equation 7 which is the gradient of the energy field [5].

$$[11] \vec{F} = \nabla(\vec{E})$$

Other Equations

Other equations utilized in coilgun designs are documented here for reference. Equations (12) & (13) are about v_{emf} which is the voltage generated on a coil of wire based on a changing magnetic field. This voltage is often referred to as back emf.

$$[12] v_{emf} = -\frac{dB}{dt}$$

$$[13] v_{emf,total} = -\frac{dB}{dt} * N$$

Equation (14) relates the voltage across an inductance (L) to changes of current or changes in inductance. Equation (14) shows that the voltage across the inductor limits the rate of current through it, as it has to wait for the derivative to reach saturation. Also, when discharged the speed of the change in current corresponds to a large negative voltage, typically called flyback or freewheeling voltage.

$$[14] v_L = L * \frac{dI}{dt} + I * \frac{dL}{dt}$$

Review of Previous Coilgun Designs

Previous designs with varying design methodologies are discussed below. This covers varying design methodologies such as reluctance vs. induction type, energy supply options, control layouts, voltage rating, and inductor sizes.

Induction-Type

With induction type designs, an electromagnetic armature is accelerated by electromagnets which pull the armature along, with the armature only becoming a magnet by the induced voltage by equations 12 and 13 [3]. These systems have a layout similar to that shown in figure 1. Furthermore, this design is asynchronous, utilizing Light

Triggered Thyristors (LTTs) as non-controlled inputs to activate these coils as shown in figure 2 [6,7].

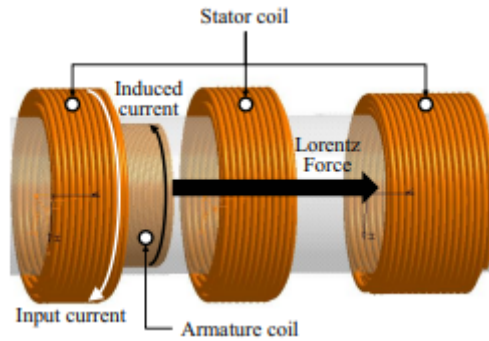


Figure 1. Side view of an induction type coilgun [6].

Figure 1 highlights the multiple stages with an internal armature also being a solenoid similar to the systems drive solenoids. Figure 2 is included to show staging between these devices as well as circuit layout with the LTTs, flyback diodes, dump resistors, and switches in the circuit as relays. Of note high voltage power supply is utilized to charge the capacitors to a supply voltage of 10kV with the capacitance per stage being 4, 2, and 2 mF [6]. With this layout and its LTTs, the system relies on the projectile to trigger the coils at each stage, making the stages asynchronous.

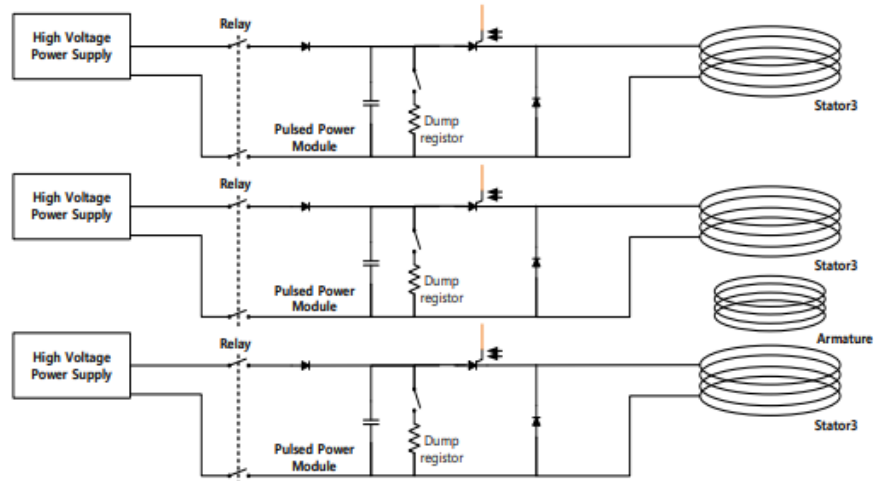


Figure 2. Schematic of referenced induction type coilgun [6].

This system is powerful, generating peak forces up to 1.3MN sufficient to move a 20kg payload up to speeds of 107m/s [6]. To supply this immense power the three capacitors were used at 10kv, with a simulated peak current draw exceeding 41kA [6]. This system also had a small number of windings on its three drive coils those being 10, 10, and 15. The armature had 35 windings [6]. Of note, this paper also highlights that to enhance efficiency the stages should be close together which is a flaw in the manufactured system [6].

Reluctance-Type

Reluctance type designs use a ferromagnetic core accompanied with electromagnetic drive coils to accelerate the armature [3]. The force generated across the core are derived from equations 3, 4, and 7. A cross section of a reluctance design is shown in figure 3 and with a circuit design given in figure 4. With this design a laminated core is utilized to minimize power loss due to eddy currents [5].

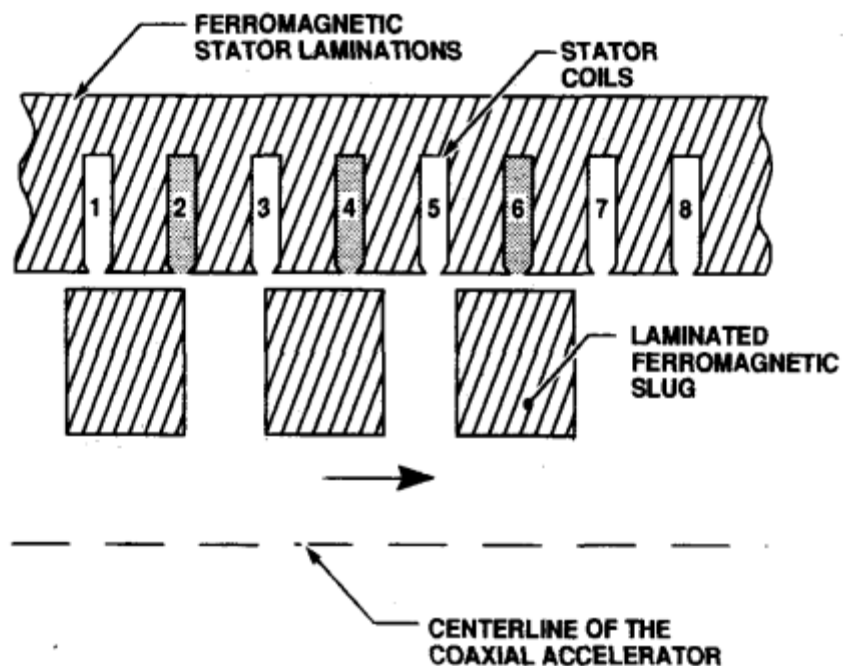


Figure 3. Side view of a reluctance type coilgun [5].

Figure 3 shows another design utilizing solid state relays (SSRs) to control the power switching and also utilizes flyback diodes to deal with the flyback voltage of the inductors.

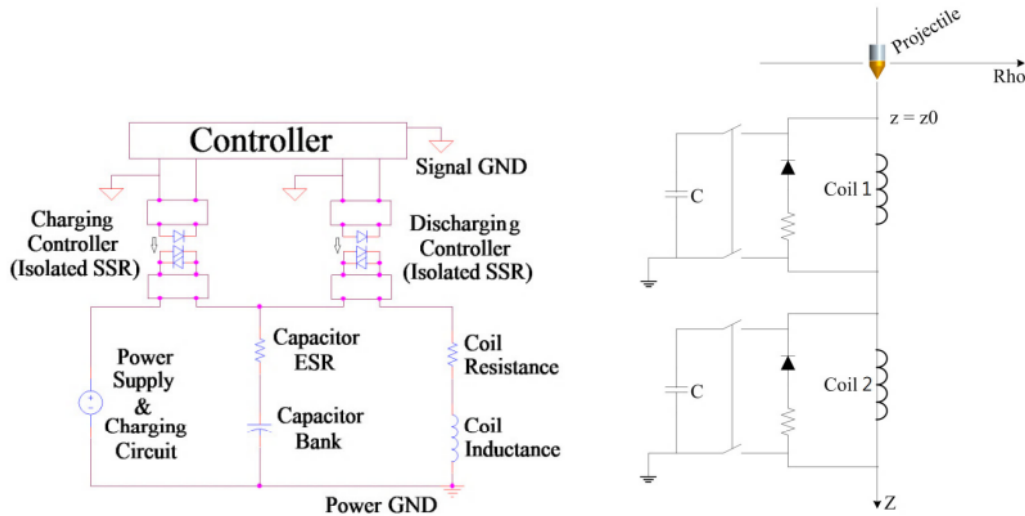


Figure 4. Schematic of referenced reluctance type coilgun [8].

This system has significantly lower current draw than the induction design with a peak simulated current draw of $\sim 5000\text{A}$ and voltage with a charge voltage of 200V [8]. To supply this system, two spot-welders were utilized as shown in figure 6. For both stages the coils were 99 turns with an armature made of a permalloy [6]. This is a synchronous design utilizing a controller to determine when the system is activated on both coils [7,8]. Furthermore, with its smaller payload $\sim 11\text{g}$ it achieved a maximum velocity of 54.84m/s [6].

Multi-Stage

Figure 5 shows the schematic of a multi-stage coilgun, which was the inspiration for our design. This configuration is a circuit that uses a photo-sensitive transistor to trigger a circuit for the multi-stage system [9]. This design was beneficial to utilize as it has a low complexity and can be made with repeated control circuits. Using these

multiple stages also helps increase the peak speed of a system through multiple acceleration periods.

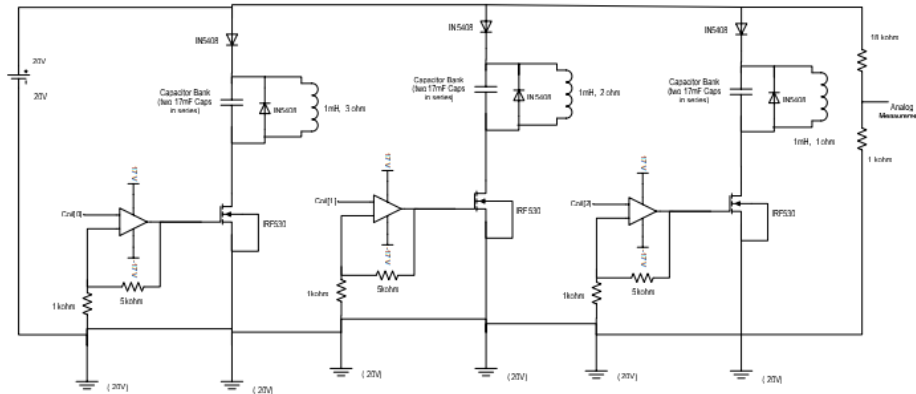


Figure 5. Referenced multi-stage type system schematic [9].

Energy Sources

Most of these systems involved high voltages and large capacitors. The exceptions were the reluctance design which utilized spot welders as shown in figure 6 and two NASA projects, each using unique technologies under magnetic energy storage [8,10,11]. Most systems that used capacitor banks like those shown in figure 7. One NASA project claimed a system with energy storage in super-conductor drive coils by using Superconductor Magnetic Energy Storage (SMES) [11]. Some designs use compulsators, these devices utilize spinning magnets and an adjustable ring to pick up the stored magnetic field [10]. Overall, the focuses on these systems are high current and high power to first generate magnetic force, and then being able to push the current through an inductance. These systems are scalable with the spot welder being one of the lowest at 200V - 5000A and the Compulsator model outputting voltages near 29kV and 1.72MA of current [10]. These operation ranges are exceptionally unique as the duty cycle for these systems are small, with some only firing for seconds and then staying off for minutes at a time.



Figure 6. Reluctance design power supply (Spot Welders) [11].

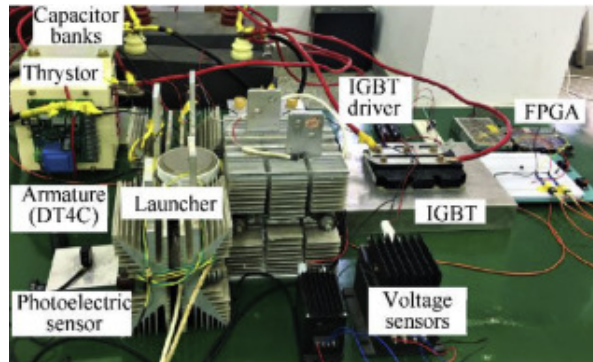


Figure 7. Coilgun Capacitor bank showcase [8].

Control Layouts

There are similarities and differences in the design of the control system. Control systems can be asynchronous or synchronous and switching can be performed with either a MOSFET, IGBT, Thyristor, or SSR. The goal is to minimize delay and be able to act when necessary whether that is feedback from an LTT or from a controller.

Advance Discharge Methodology. One common feature in the induction and reluctance designs is that of flyback diodes. One idea to enhance performance of coilguns is to enhance the efficiency of this component by switching to a synchronous discharge design. The idea of synchronous switching is utilized in power converters like H-bridges to enhance performance. The concept of synchronous discharge was also tested with coilguns and enhanced efficiency with incremental efficiency of up to 36.34% with a circuit layout shown in figure 8 [12]. Furthermore, as the voltage increases the designed discharging circuit performed better, as documented in table 2 [12].

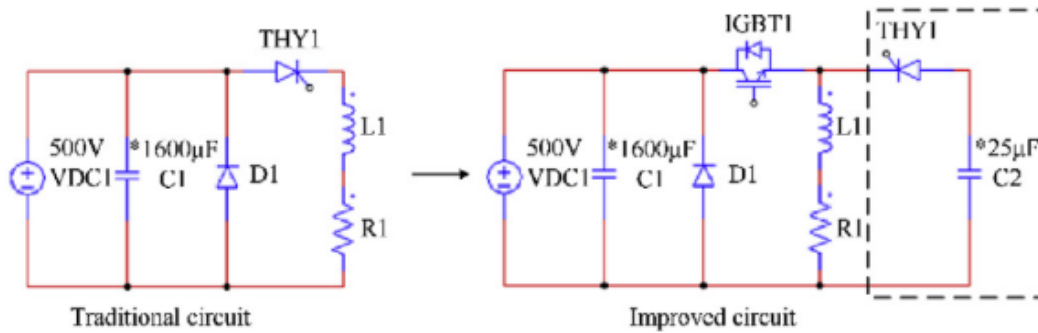


Figure 8. Concept of synchronous switching discharging circuit [12].

Simulated results of different voltages with traditional circuit and improved circuit.

Voltages/ V	Velocities with traditional circuit/ (m·s ⁻¹)	Velocities with improved circuit/ (m·s ⁻¹)	Efficiency of traditional circuit	Efficiency of improved circuit	Increment of efficiency
500	7.90	8.24	5.25%	5.75%	9.11%
600	9.29	10.05	5.06%	5.94%	17.39%
700	10.48	11.74	4.74%	5.95%	25.53%
800	11.50	13.34	4.37%	5.89%	34.78%

Table 2. Simulated data from advance discharge circuit [12].

Solenoids

Solenoids or drive coils are the main generator of the magnetic force used in coilguns for both induction and reluctance type designs. The reason for their importance is that they generate the magnetic flux density, or the flux experienced by the armature, which directly translates into force through equations 3, 7, 9, and 11. Their involvement with those equations is due to the curl of their magnetic fields across the gradients in

equations 7 and 11. With the great correlation between field of the solenoid to its force produced the shape becomes most significant from equation 3. To understand how the shape of the drive coils affects the force, two studies were analyzed. One is concerned with axial manipulations of S_a , L , and V . The other is concerned with radial manipulations, effectively how manipulating the S_r changes the force of a solenoid.

Solenoids typically have an extremely non-linear force curve. A typical force curve is shown in figure 9. A positive force peak occurs well before reaching the center of a solenoid. Furthermore this force curve is related to the change of the field, specifically the flux generated by the solenoid as figure 10 is correlated to figure 9.

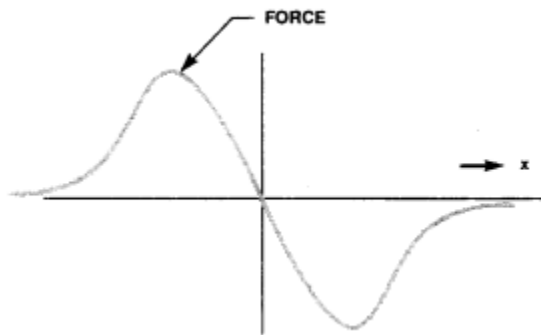


Figure 9. Example force curve (\vec{F} vs. displacement $\{x\}$) across a typical solenoid [5].

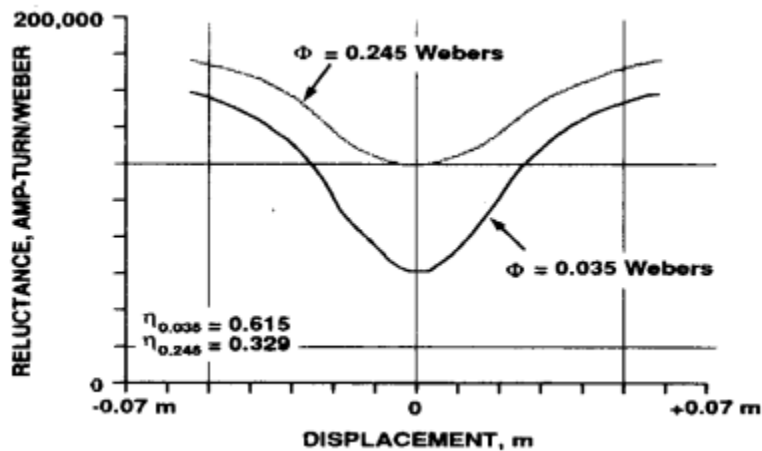


Figure 10. Example curve of reluctance/field across a solenoid [5].

Figure 10 highlights the field fluctuation across the displacement of a solenoid. The force as shown in figure 9 is related to the field through its derivative. This relationship between the field and the force is shown by equations 7 and 11. To optimize force over distance, the armature needs to receive a constantly changing flux across the majority of its distance.

In addition to manipulation of force, another unique issue with these devices is that they are susceptible to fluctuations in inductance of the solenoid as shown with a reluctance-based design shown in figures 11 and 12. This change in inductance generates EMF as the inductor tries to resist changes in the magnetic flux. This is described by equations 12, 13, and 14. So, another issue entirely of these systems is the “fight back” from induced emf and voltage on an inductor.

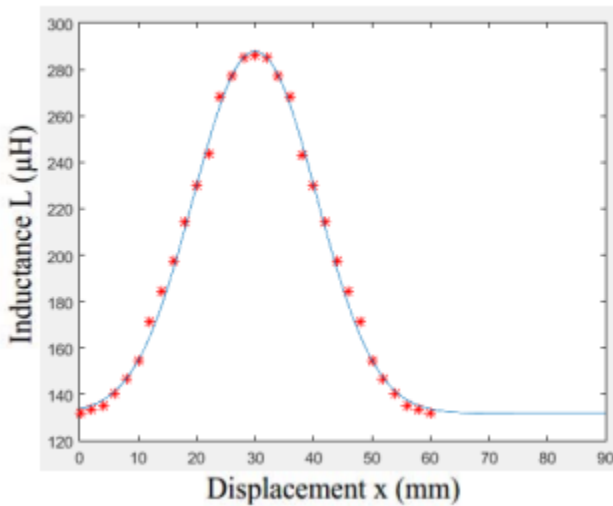


Figure 11. Variation of inductance of drive coils during launch [13].

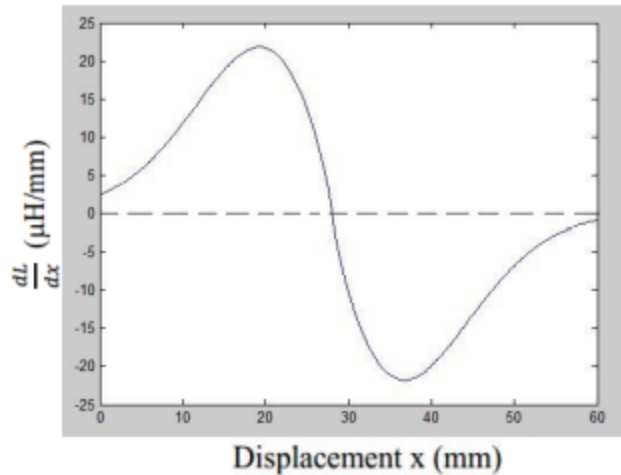


Figure 12. Derivative of inductance of drive coils during launch [13].

Axial-Shape Manipulations

With research concerned with peak force, a study focused on the varying axial length of a solenoid while maintaining the total wire length constant [14]. These changes cause the number of turns, axial cross section, and solenoid volume to fluctuate. This is illustrated in figures 14 and 15, with respect to a 3m long wire. The shape of these variations is shown below in figure 13 with length (l), inner, and average diameters (d_i, d_a). When winding solenoids, the wire will sit on top of each other as shown in figure 13.

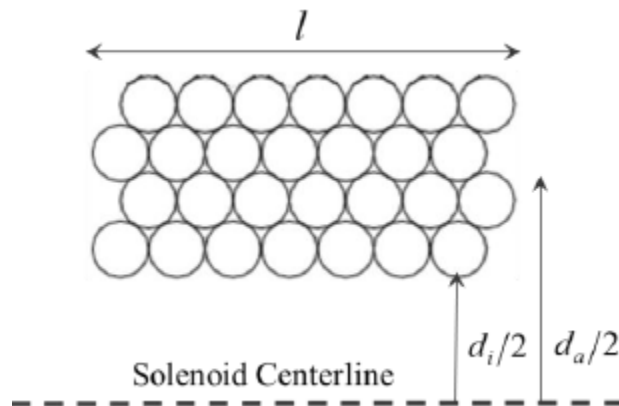


Figure 13. Solenoid cross section for axial manipulations [14].

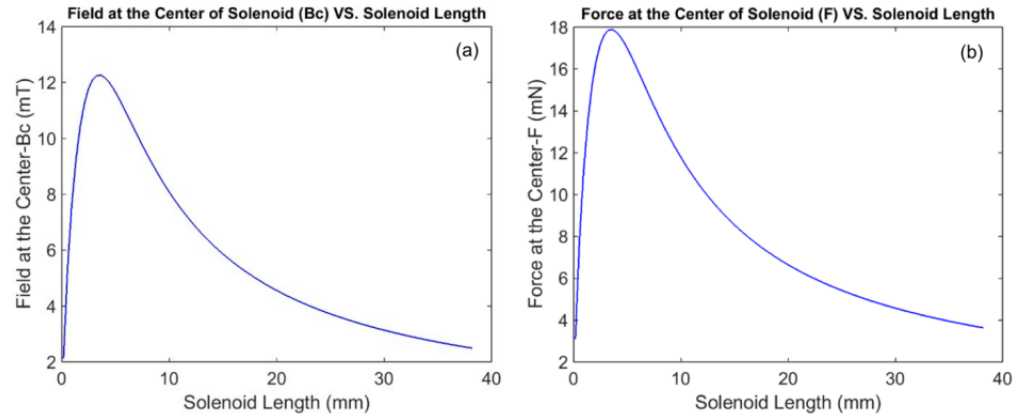


Figure 14. Field (a) and force (b) of a solenoid as length is varied [14].

Figure 14 shows how the concentration of the field and peak force fluctuates as a function of the solenoid length. This shows that equation 1 does not account for geometrical properties of solenoid design, as with longer solenoids if the force decreases too much the projectile will never exit because of the static friction. From these plots it can be determined that turn, or Ampere turn, density causes the fluctuations of force [14]. The main reason for the increase in force is shown in figure 15. At a certain length there is an optimum amount of turns within the solenoid volume, specifically 215 [14]. Figure 15 is a comparison to the number of turns as solenoid length changes.

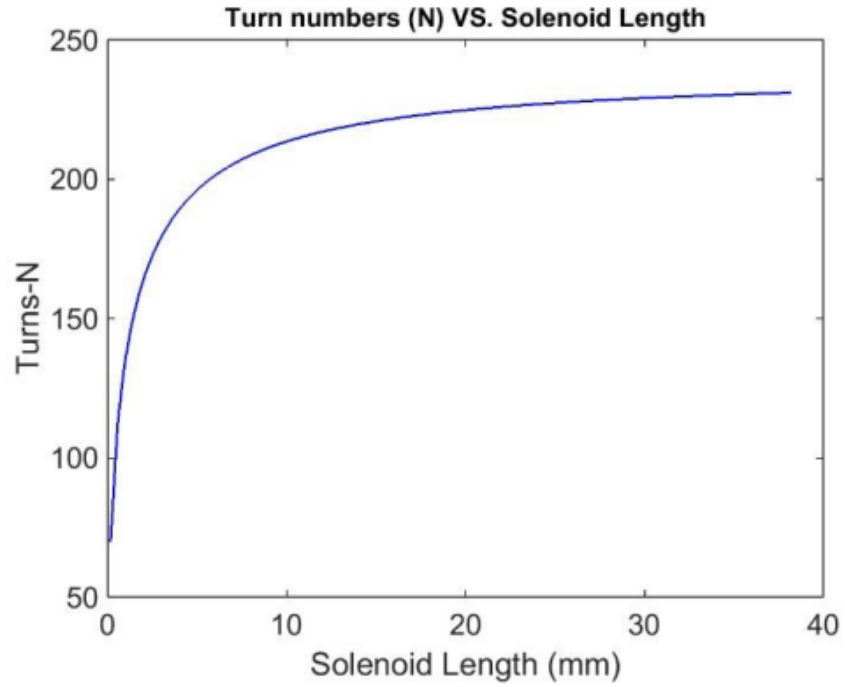


Figure 15. Number of turns of a fixed length wire solenoid as length increases [14].

Figure 15 shows that the turns of a a solenoid grow logarithmicly based on the length of the solenoid. However, the optimum point as shown in figure 16 is not at the maximum number of number of turns, rather at a maximum number of turns at a shortest solenoid length.

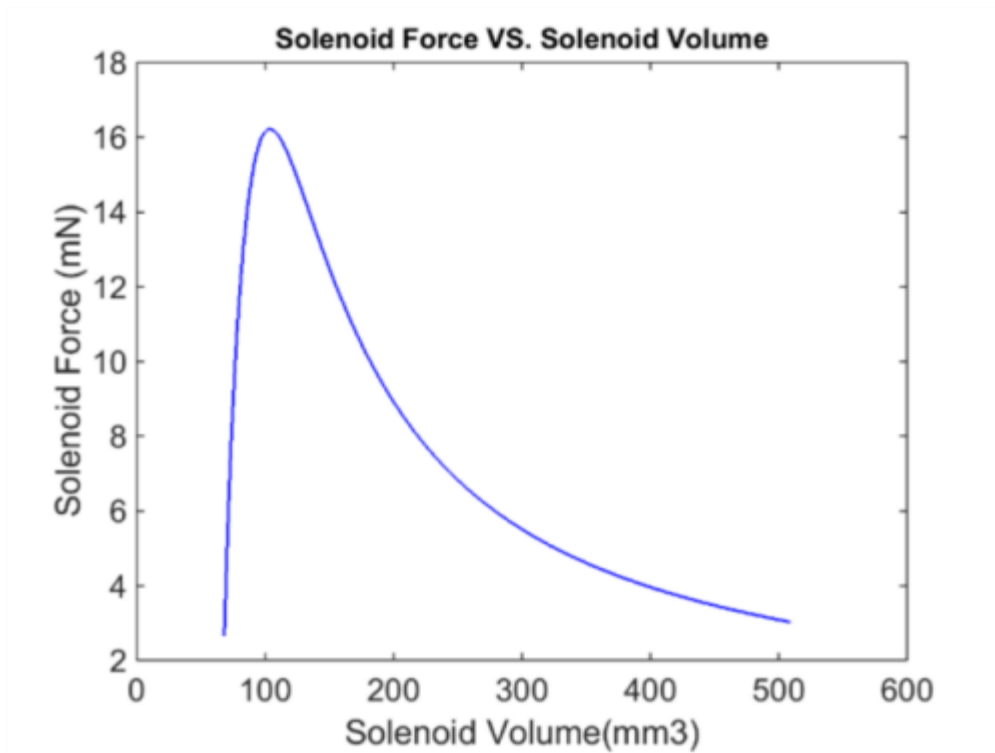


Figure 16. Force generated by a solenoid as volume fluctuates [14].

As shown in figures 14(B) and 15, the optimum point is related to the turn density. Furthermore, figure 16 highlights this, as the optimum force occurs at a small volume. To optimize a solenoid design, the focus should be on compacting the volume while maintaining a maximum number of turns within its volume (N). This increased turn density when applied to equation 3 correlates to a more intense field strength.

This study also took the data from the above plots and tested it on various wire lengths and wire gauges [14]. The results of these changes are that the length of wire greatly affects force, power consumed, and optimum length. Wire gauge also manipulated the same parameters but was mostly concerned with resistance and allowable current.

<i>Wire Length (lw)-m</i>	<i>Optimum inner dia. (di)-mm</i>	<i>Optimum coil length (l)-mm</i>	<i>Consumed power (P)-Watt</i>	<i>Force to cross-section ratio (F/A)</i>	<i>Force to cross-section to power ratio (F/AP)</i>
1	1.85	5.29	0.0932	325	3.48×10^3
2	2.98	5.85	0.1864	541	2.90×10^3
3	3.69	6.44	0.2797	662	2.37×10^3
4	4.39	6.91	0.3729	756	2.03×10^3
5	4.82	7.39	0.4661	827	1.78×10^3

Table 3. Optimum solenoid parameters based on wire length [14]

Table 3 shows how optimum solenoid length and inner diameter change as wire length is changed [14]. With the data above the length of the coil can be used to determine the optimum inner diameter which is usually fractional, with the data above leading the inner diameter to be 0.349 to 0.652 the length [14]. From the given optimum outer diameter of 1.51 times greater than that of the inner diameter [14].

Table 4. Optimum solenoid parameters based on wire gauge [14]

Table 4 gives the relationship between wire gauge and optimum length [14].

Radial-Shape Manipulations

<i>Wire Gauge</i>	<i>Wire dia. (dw)-mm</i>	<i>Resistance/length- (mΩ/m)</i>	<i>Allowable current-A</i>	<i>Optimum inner dia. (di)-mm</i>	<i>Optimum coil length (l)-mm</i>	<i>Force to cross-section to power ratio (F/AP)</i>	<i>Force to cross-section ratio (F/A)</i>
34AWG	0.160	856	0.33	3.7	6.4	2.36	0.66
36AWG	0.127	1361	0.21	3.1	5.6	3.04	0.55
38AWG	0.101	2164	0.13	2.7	4.8	3.99	0.44
40AWG	0.0799	3441	0.09	2.3	4.1	4.65	0.39

With solenoid designs the side profile or radial cross section is another point of interest as by changing the number of turns across the solenoids length the force curve can be manipulated. These manipulations are used for linearization of the force curve as shown in figure 21 when compared to figure 9. With this two prior works are discussed one involved with radial modifications of the armature and the other with radial modifications of the coil housing. Additionally, no works were found concerned with changing the shape of the coils.

Radial Manipulations of Armature

One method to optimize force output of a solenoid is to use multiple coils, but this solution leads to high peak forces across the displacement of the armature. An example of such a system is shown in figure 17. The unmodified model showcased uses a rectangular armature and has large peak forces as shown in figure 19 [15]. The optimized solution shown in figure 18 used a modified cross section on the armature to have a desirable force curve as shown by the darker line in figure 19. This may be beneficial to systems as some peak accelerations may exceed 33000 Gs of acceleration [2].

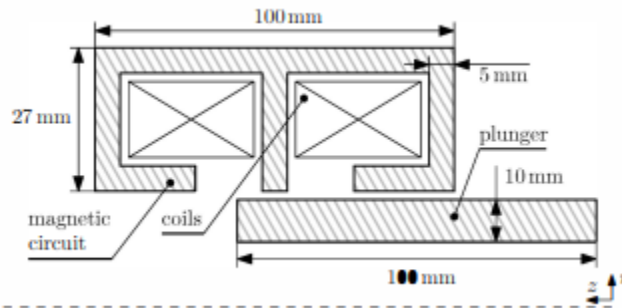


Figure 17. Initial State of Radially Modified System [15].

Figure 17 shows the initial state of a two coil system before the armatures radial cross section (S_r) is modified [15]. This is for comparison of how much material is removed from this method, as shown below in figure 18, with optimized geometry [15].

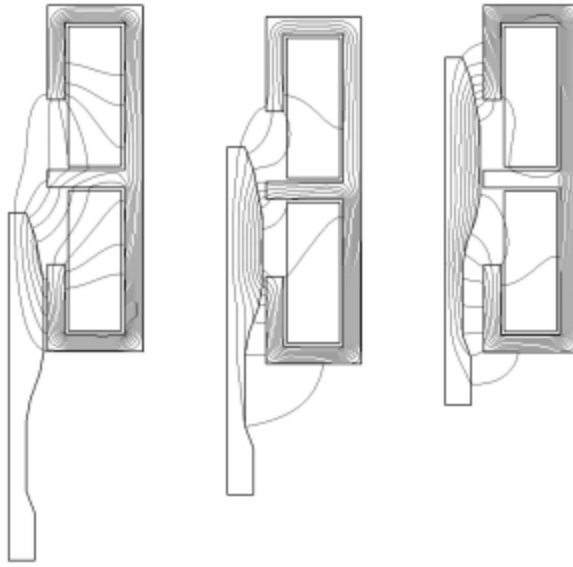


Figure 18. Final state of radially modified system [15].

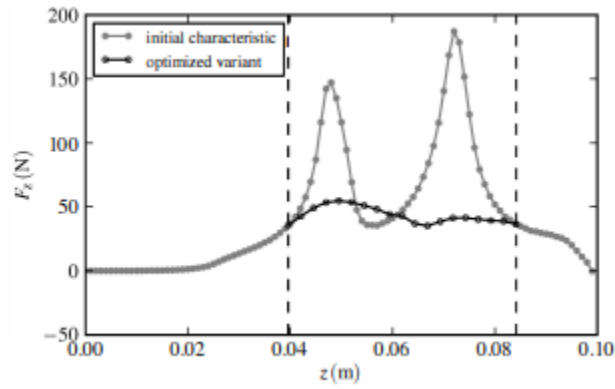


Figure 19. Results of geometrical optimization of armature [15].

These results show that in exchange for linearizing the force curve maximal force is reduced, losing overall exit velocity. This concept may be utilized in other designs to highlight potential benefits of armature geometry optimizations, however reducing the material of the armature reduces the peak force which makes the system undesirable for solenoid-based accelerators.

Radial Manipulations of Coil Housing

For radial manipulations, there are two places for changes, that of the drive coil itself or that of the magnetic material around the coils. The magnetic material around the coils is that of the magnetic yoke which is the red material in figure 20, the blue material maybe magnetic but it is not stated directly. Instead it is called the guider and serves as smooth sliding surface [23]. There were no documents about coil manipulations directly but manipulations of the magnetic yoke should yield performances due to their conduction of magnetic fields. The methods given coils or magnetic yoke utilize changing the direction of the field by equations 3,7, or 11 to generate unique force curve solutions. To start with the radial manipulations, the first as shown in figure 21 is that of W , the thickness of the guider as shown in figure 20. This change had a positive effect on peak force as it is increased.

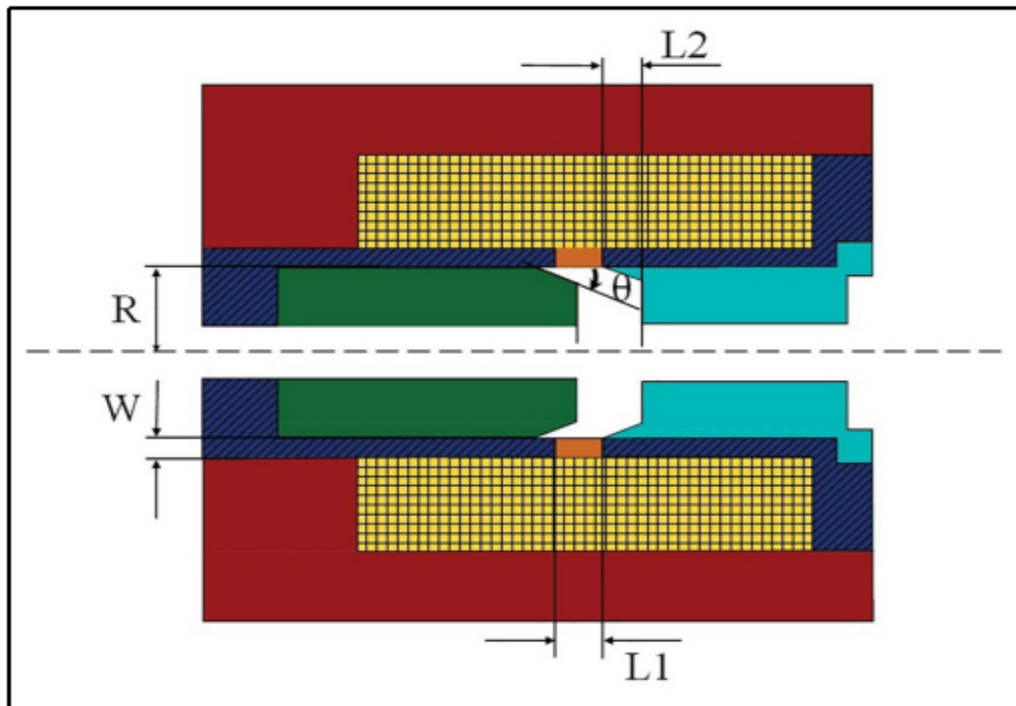


Figure 20. Solenoid armature and coil parameters for radial changes [16].

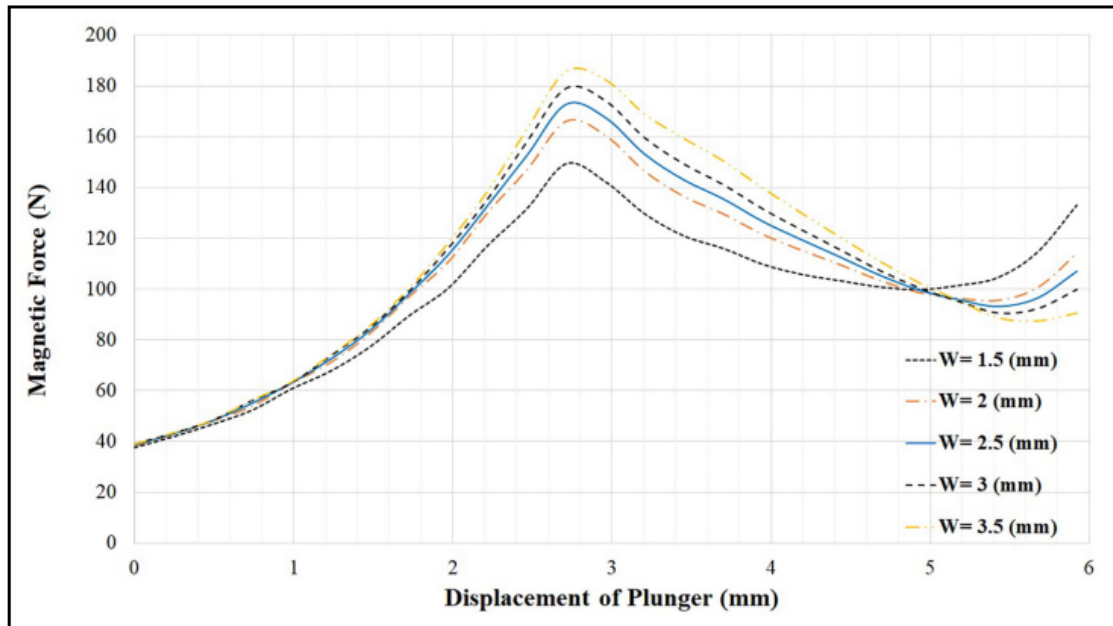


Figure 21. Force response to solenoid guider thickness (W) variation [16].

As guider thickness increases, force increases, but will eventually saturate. Other manipulations such as $L1$, $L2$, and θ did induce some changes. $L1$ did not add much as it changed, in contrast $L2$ and θ both had fluctuations of $\sim 40\text{N}$ in their ranges leading to magnetic material manipulations having great impacts on the force [16].

In addition to manipulations of the magnetic material around a coil, there are the geometrical manipulations of the coils. This is the purpose of the MATLAB simulations described in the next section. An example of a horn shape for the radial profile is shown in figure 22. Levi Janssen proposed this idea but did not test it. He believed with a longer solenoid as pictured would have too weak a field to accelerate objects [17]. However, based on the equations this long region generates a longer region of acceleration due to a longer lasting gradient of field as it tries to concentrate down the bore. This longer region of acceleration may lead to heightened performance whether that is velocity per stage or efficiency per stage.



Figure 22. Concept of non-cylindrical drive coils for coilguns [17].

MATLAB Simulations

To understand how the radial cross-section affects coilgun performance, a simulator was generated to make a realistic model of a solenoid winding across an axis. This simulator does not iterate to determine the best solution, rather it generates the field of the solenoid windings and takes the gradient of the B field to determine if there is a considerable gain to peak force and what shapes best alter the center of the solenoid force towards the end.

The goal of this is to see if one of these designs help minimize the negative force of the solenoid that generates when the solenoid is deactivated or generate a wider acceleration region to boost top speed. The parasitic effect of solenoid deactivation plagues these systems due flyback, as the inductances cannot discharge fast enough. Furthermore, manipulating the acceleration region may lead to enhanced performance either by having the solenoid for a shorter time by condensing the acceleration region or a longer time by expanding it. The main question is if the region with opposite force direction is minimized will the pushback force drop, or maintain more velocity? This pushback force is shown in figure 23. The velocity loss is extrapolated from the

discharging circuit details of figure 8 and its data in table 2, as well as being shown in figure 23.

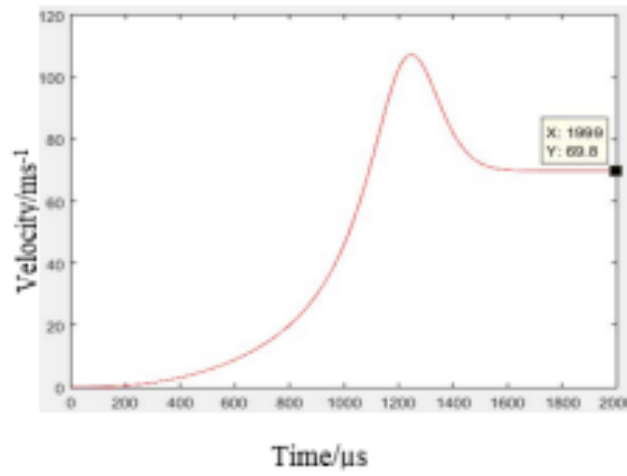


Figure 23. Velocity Loss at Solenoid Discharge [13].

At solenoid discharge there is a velocity loss on the projectile, what this comes from is solenoid being slow when discharging.

Code Documentation

The code utilizes a MATLAB based Biot-Savart Law simulator to generate the field of a given shape [19]. The shape is generated by using the alphashape function to generate a radial cross section and generates the shape based on wire size and how many shapes can fit within the cross section. Then the 3d field around the drive coils is generated, based on some system parameters. The current and voltage parameters are entered at the start of the program and can be iterated based on the calculated resistance of the coil with the system.

Simulation Results

A control solenoid was generated by using the information documented in tables 3 and 4. With interpolation the data an 8-layer solenoid with 240 turns was generated. The shape was based off the selected wire gauge, 20AWG, and interpolated off of the wire's cross-sectional area from table 4 resulting in a length of 25.10mm. Then with that length, the optimum inner diameter was estimated to be 15.72mm, and an outer diameter of 26.88mm. With the generated cross section, the height of the solenoid was estimated from the data to be 7.09mm. The data was used to generate the solenoid shown in figure 24, with its field curve in figure 25.

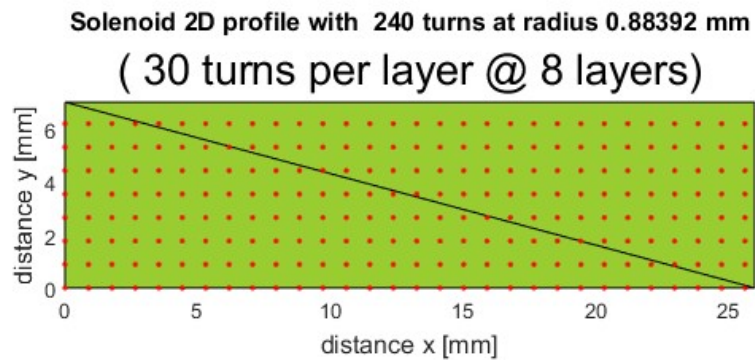


Figure 24. Control solenoid cross section profile.

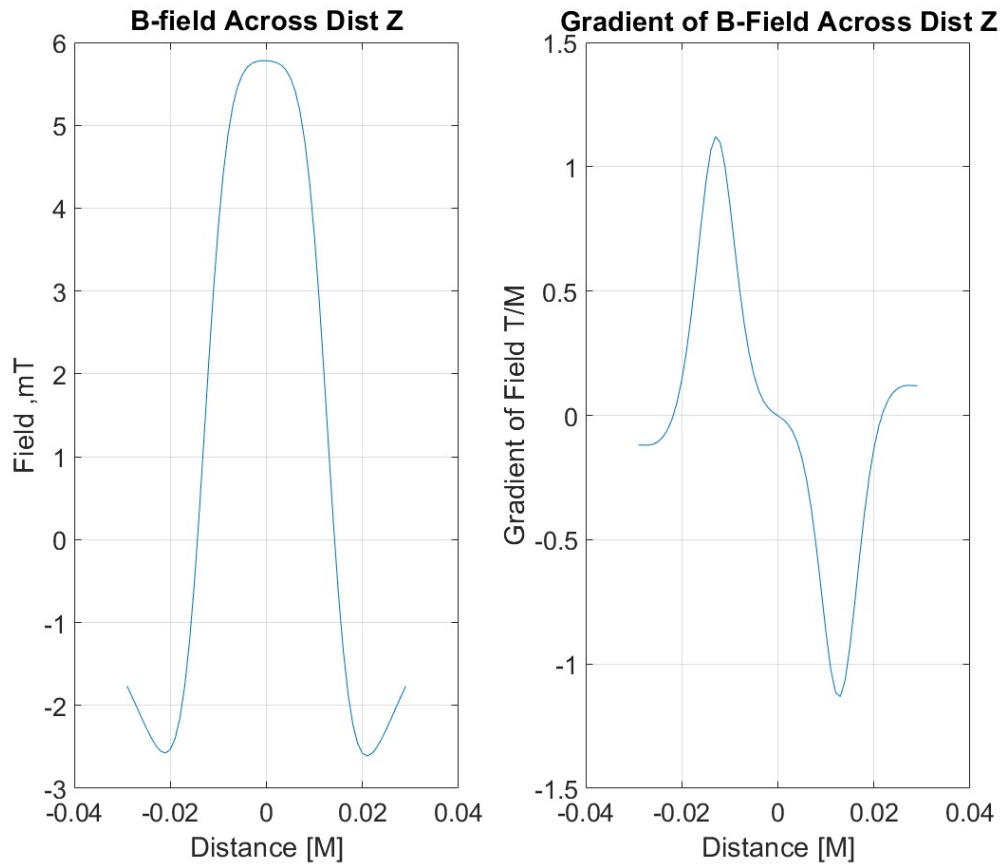


Figure 25. B-field (a), gradient of B across z (B) of control solenoid.

Figure 25 shows the control solenoid's field is nearly uniform resulting in an even gradient and balanced field gradient about the solenoid's center. For the second design, a triangular shape was added to the cylindrical model while maintaining the same number of turns. Its cross section is shown in figure 26 and its field in figure 27. This change shifts the center of the field towards the further end of the coils, allowing for a wider acceleration region and narrower opposing region.

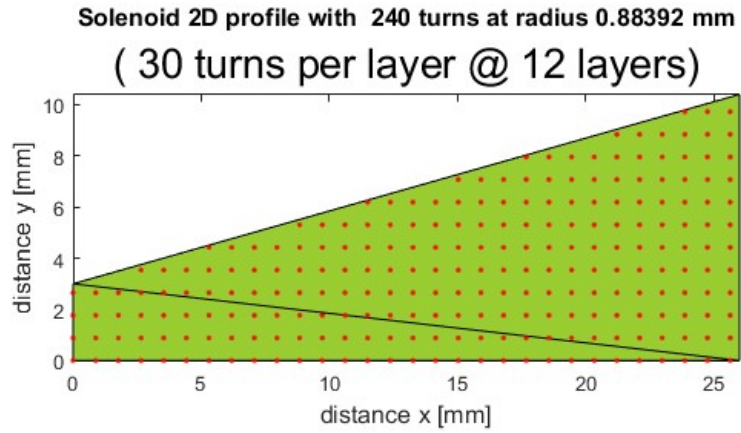


Figure 26. Triangular solenoid cross section profile.

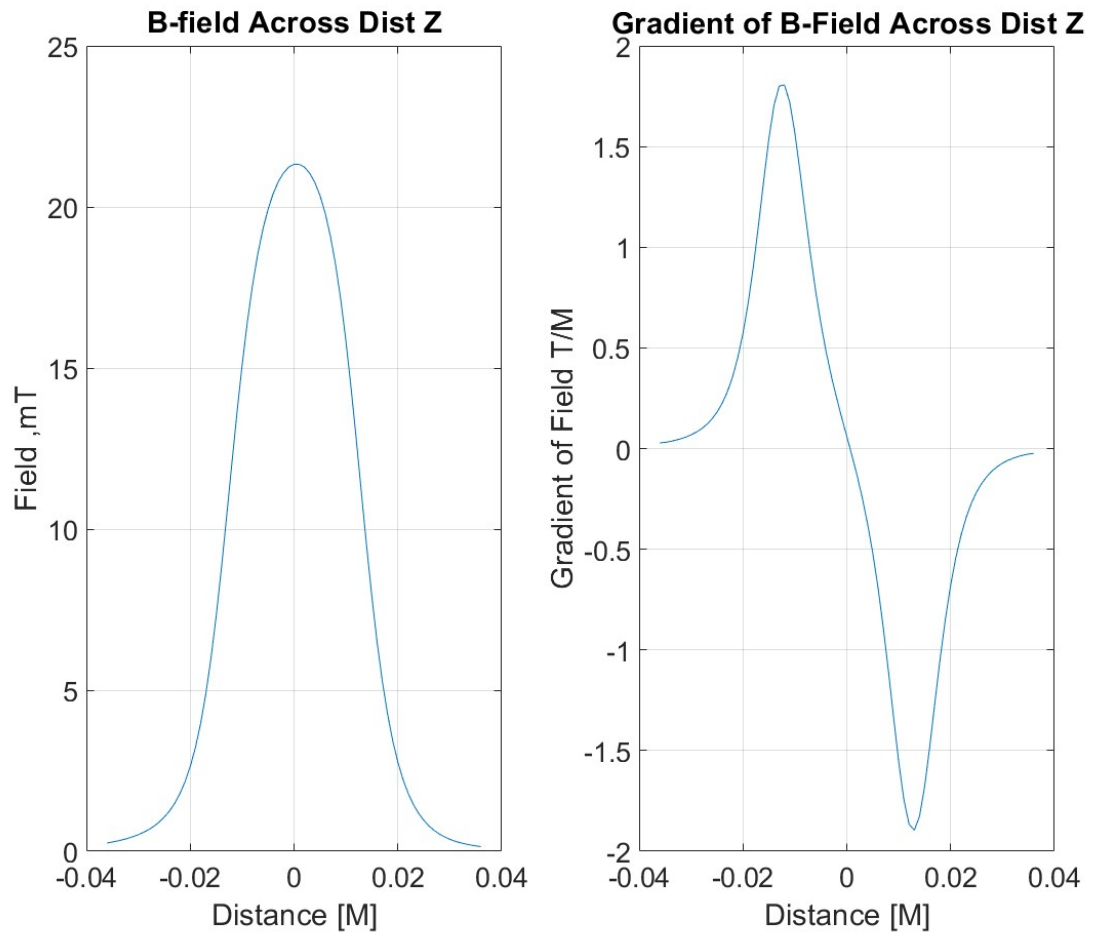


Figure 27. B-field (a), gradient of B across z (B) of triangular solenoid.

For the third design a horn shape was tested to see a more heavily sloped side changes performance significantly. The solenoid shape is shown in Figure 28 resulted a unique field shape as shown in Figure 29. This lopsided shape may be beneficial as using the shorter acceleration side may be good at boosting efficiency by reducing on time with higher peak force, and the longer side could be better for allowing for more time under force.

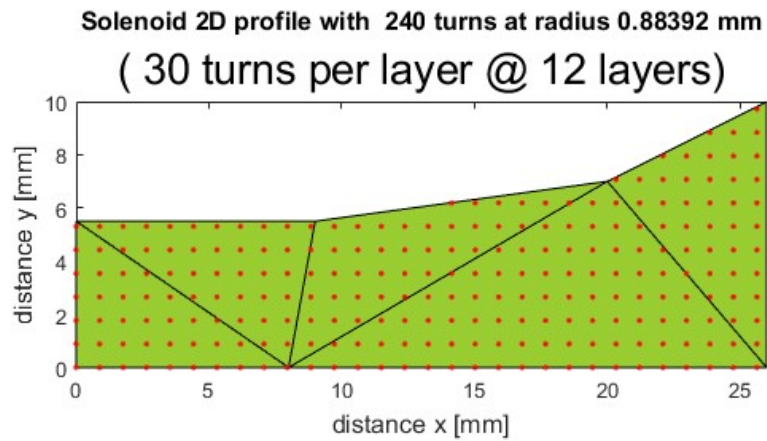


Figure 28. Horn solenoid cross section profile.

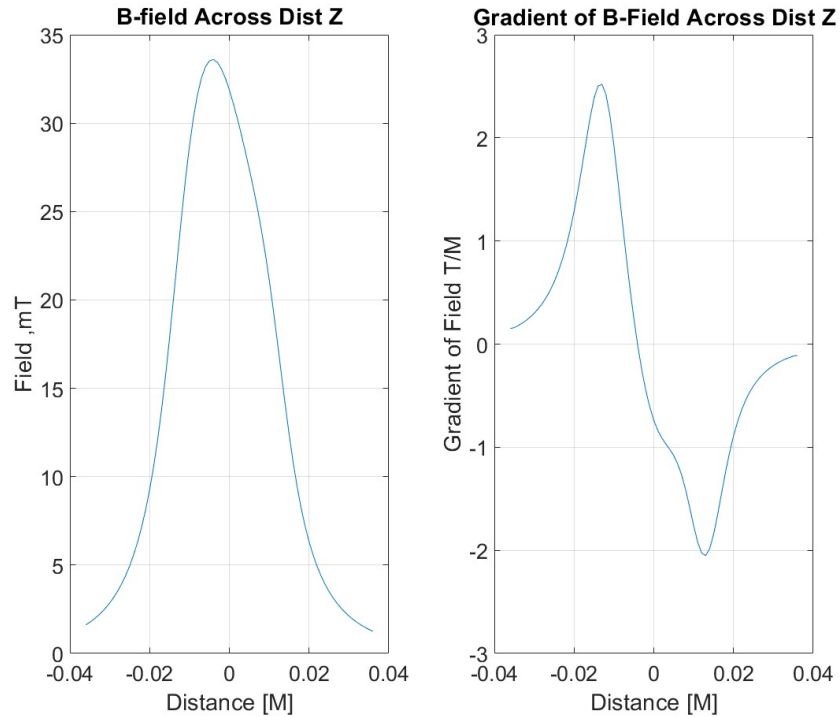


Figure 29. B-field (a), gradient of B across z (B) of horn solenoid

Experimental Testing

For experimental testing the three solenoid shapes mentioned in the simulations section were utilized. The housings for these were 3D printed and tested with hand wound solenoids.

System

The system designed for experimentation is a low-voltage coilgun to reduce risk of electrical shock. This also allowed the system not to require enclosures to protect against arcs. Furthermore, the low voltage allowed to use a more inexpensive capacitor bank. The design was based upon the reluctance design given earlier, with a maximum capacitor bank voltage of 50V, peak output current capacity of ~40A, four stages, and a bore diameter of 3/8 inches designed to launch various magnets under 0.25in. Relevant

data for this design has been put in Appendix B as well as documented on a public GitHub page.

There were two iterations of the coilgun. The first was a development coilgun which granted insight into various system design issues. The problems were resolved on the second iteration by maintaining signal integrity with a shielded DB9 bus, bypass & decoupling capacitors to reduce signal noise, and shielding and ground management.

Testing Procedure

The procedure of testing the solenoids as follows:

1. measuring tested solenoids inductance, resistance, quality factor, reactance, and impedance. Results documented in tables 5,6,7
2. start with 4 stage solenoid launching and measure speed with E9800-x chronograph 5 times @ 50, 45, 40 volts
3. square solenoid launching 5 tests @ 50V
4. Triangle solenoid launching 5 tests on 2 coils @ 50V
5. Horn solenoid launching 5 tests on 2 coils @ 50V

For each launch the test procedure was as follows:

1. Load armature to position marked before solenoid backing
2. Ensure E9800-x is active and 5v control system (LEDs on)
3. Charge capacitors to voltage
4. Document charged voltage of capacitors
5. Fire system
6. Document remaining capacitor voltage
7. Read E9800-X reading

Of note the armature was not modified between different solenoid shapes as to ensure they were consistent with testing, if this was modified there may also be performance gains.

Experimental Results

The measured results of the three solenoids (control, triangular, and horn shaped) are shown in tables 5-7 and figures 30-34. The measured test data and code for plotting is documented in Appendix C. All tests were performed on the second coilgun iteration.

Parameter	Value
L	709uH @1kHz
Q	7.25 @1kHz
R	615.15mohm
X	4450 ohm
Wire	20 AWG
N	240 turns
Length	25.1mm

Table 5. Measured parameters of control solenoid.

Parameter	Values
L	733/726uH @1kHz
Q	7.6/7.15 @1kHz
R	609.114/638.177mohm
X	4606/4562ohm
Wire	20 AWG
N	240 turns

Length	25.1mm
--------	--------

Table 6. Measured parameters of triangular solenoid.

Parameter	Values
L	692/646uH @1kHz
Q	7.35/7.07 @1kHz
R	592.21/574 mohm
X	4349/4063 miliohm
Wire	20 AWG
N	240 turns
Length	25.1mm

Table 7. Measured parameters of horn solenoid.

The first test was of a four-stage system with all square coils. This test documents the added velocity of multiple stages and heightened charge voltage. Figure 30 shows the velocity at various charge voltages, and Figure 31 shows the efficiency at these voltages.

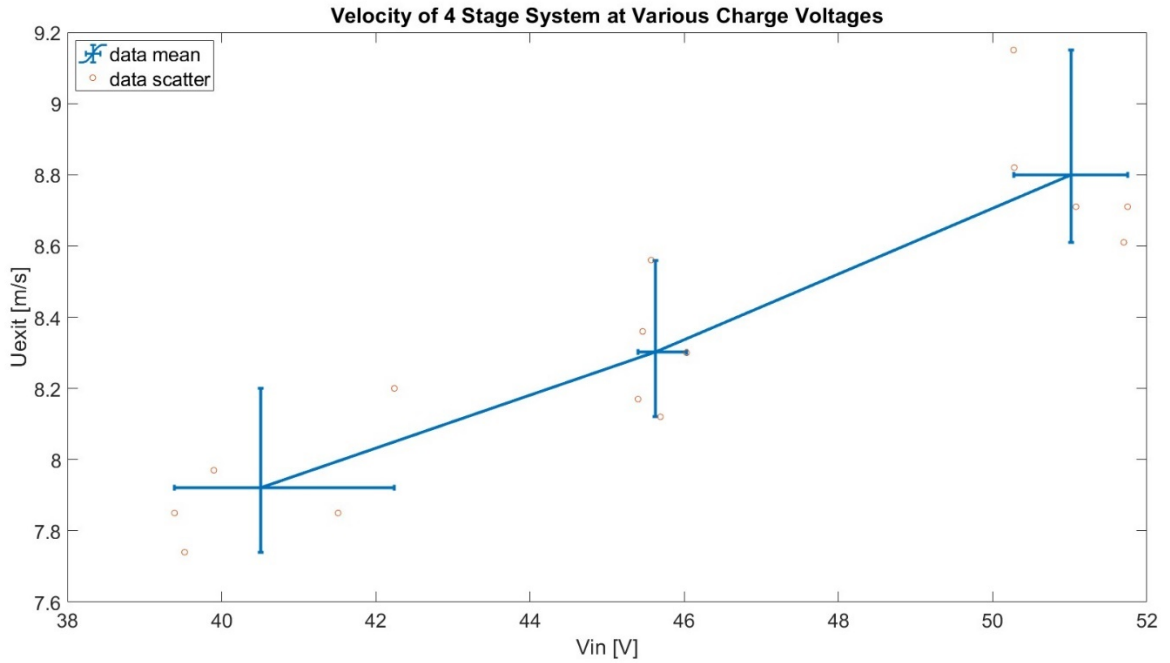


Figure 30. Velocity (U_{out}) of system as a function of charge voltage.

Figure 30 shows as the charge voltage increases, the exit velocity increases, though the increase is at a shallow slope of $0.074 \frac{m/s}{V}$. This shows a large voltage increase is necessary in order to gain considerable speed, especially up to the 11km/s [2].

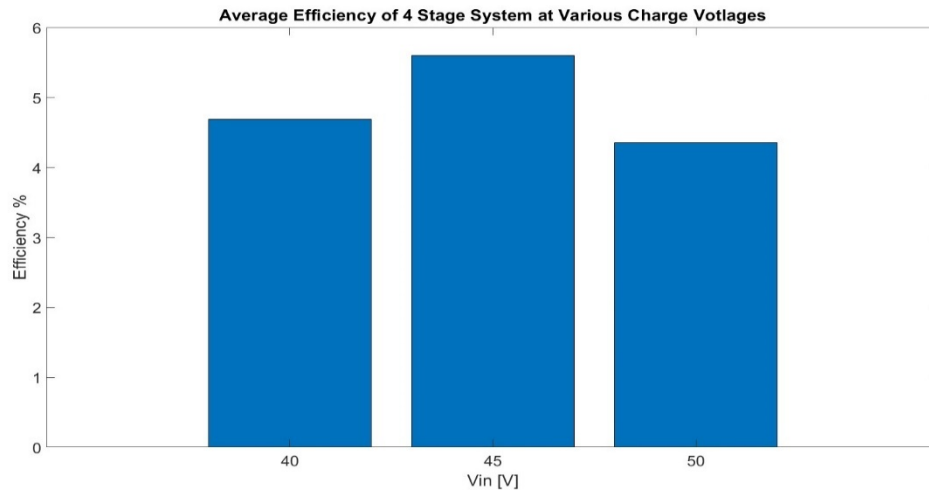


Figure 31. Efficiency average of system across charge voltages.

Figure 31 shows the average efficiency as a function of the charge voltages. The 45-volt charge had the highest performance, though the other values are not vastly lower, 45 was at 5.60% while 40 and 50 were at 4.69% and 4.35%.

For the three solenoid shapes the exit velocities and efficiency of each are shown in Figures 32 and 33. Figure 32 showcases the minimum (<), average, and maximum(>) velocities for each solenoid tested. Labeled as square for the control, T as triangle, and H for horn.

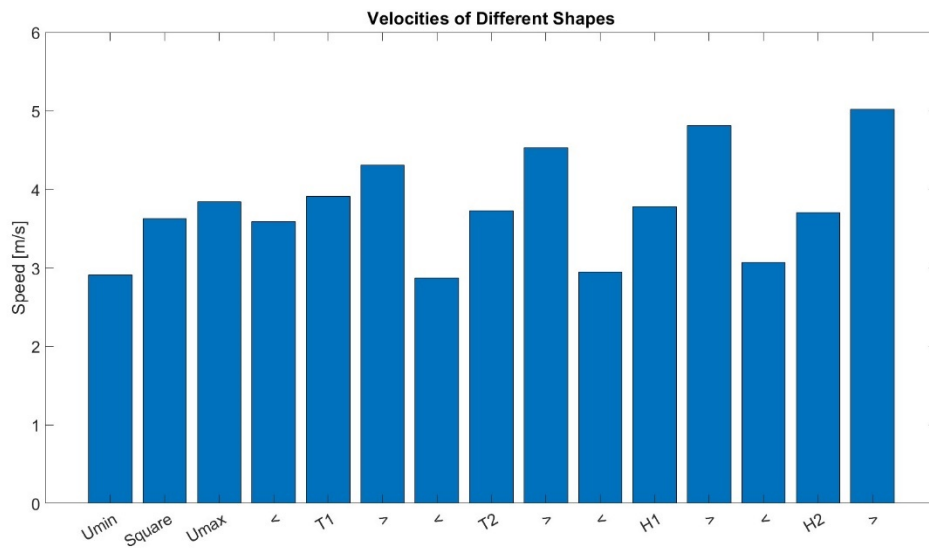


Figure 32. Minimum, average, and maximum velocities from drive coil shapes.

Figure 32 shows the measured velocities of drive coil shapes. The triangle shape was the most consistent in its velocity, and the horn shape has the highest overall velocity at 5.02m/s, compared to the triangles 4.81m/s or controls 3.84m/s. The actual values for the measurements are documented in the code for Appendix C.

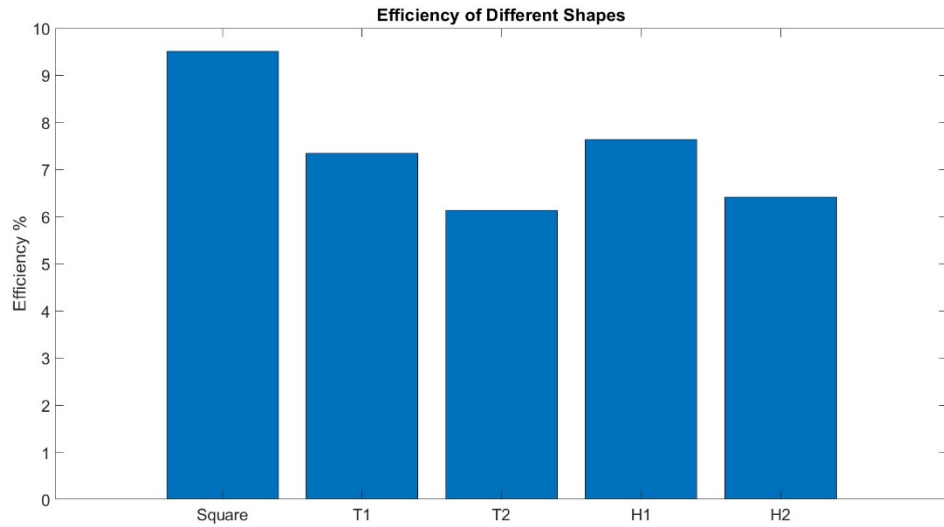


Figure 33. Efficiencies from different drive coil shapes

The efficiency has found to decrease with these new shape designs even though the velocities increased. This is shown in Figure 35. The control performed the best at 9.51% as compared to the triangles at 7.34% and 6.13% or the horn shaped at 7.63% and 6.41%.

DISCUSSION

By modifying the solenoids radial cross section, there are performance changes. For a single stage coilgun, modifying the coil's shape results in higher velocities as shown in table 7. However, the higher velocity comes at a reduction of efficiency. There are potential modifications to boost performance, such as armature manipulations or advanced discharge circuits. The results below show that modifying the shape of a solenoid can enhance the velocity performance of the system. In addition, the tests were not ideal as position of the armature on the barrel was done by hand, and the armature may have worn from repeated impacts after launch.

Shape	Velocities (min, avg, max) [m/s]	Efficiency [%]
Square	2.91, 3.63, 3.84	9.51
Triangle 1	3.59, 3.91, 4.31	7.34
Triangle 2	2.87, 3.72, 4.53	6.13
Horn 1	2.95, 3.78, 4.81	7.63
Horn 2	3.07, 3.71, 5.02	6.41

Table 8. Calculated results of various solenoid shapes

From this testing, a square solenoid gives good performance with a consistent velocity and great efficiency. Though alternative shapes provided a heightened velocity from a single stage, this was at the cost of efficiency and consistency. Additionally with the large distance of the velocity measurement and launching stage, nearly 6ft, the gains of the alternative shapes may have been higher. Furthermore, changing armature lengths may cause more desirable reactions based on the switching point of the control system. Additionally, the wide dispersion of velocity on the alternative shapes shows that they

become more sensitive to initial position. With the horn shape having the highest maximal velocity of 5.02m/s, the field shape condensed to the entry side has better performance. This is duplicated with the triangular solenoid however not as significantly. This gain is theorized to come from the switching of the solenoid occurring in this lowered gradient area. Furthermore, the higher peak gradient of the horn shape versus the triangular shape also aligns to a higher peak speed with the higher force applied.

CONCLUSION

The measured results show that altering the shape of the solenoid can generate a measurable performance change. Though, without manipulating the armature of the system, these performance changes caused a velocity gain with a significant efficiency loss, on average of 2.63%. Simulations, of various designed solenoid shapes show that alterations the geometry of the device plays a role in their field distributions and force curves. With these shapes it is possible to generate force curves with having asymmetric field curves which proved advantageous to increasing system velocity. The gain of velocity is due to manipulations of the field emitted by the solenoids in the SBA by having shifted or asymmetric field concentrations or gradients allowing the switching of the system to have a higher velocity. Implementing the manipulations of the discharging circuit, armature, and solenoid axial and radial optimizations a system can be generated that has higher performance.

BIBLIOGRAPHY

- [1] B. N. Turman and R. J. Kaye, "EM MORTAR TECHNOLOGY DEVELOPMENT FOR INDIRECT FIRE." Sandia National Laboratories, Albuquerque, Nov. 1, 2006
- [2] J. M. Schroeder, J. H. Gully, and M. D. Driga, "Electromagnetic launchers for space applications," *IEEE Transactions on Magnetics*, vol. 25, no. 1, pp. 504–507, 1989, doi: <https://doi.org/10.1109/20.22590>.
- [3] "Optimization of reluctance accelerator efficiency by an improved discharging circuit," *Science Direct*, 2020. <https://doi.org/10.1016/j.dt.2019.08.013> (accessed Mar. 04, 2024).
- [4] J. Holzgate, "Effect of Projectile Design on Coil Gun Performance," Thesis, Franklin W. Olin College of Engineering, 2012. Accessed: Mar. 25, 2024. [Online]. Available: <https://pdfcoffee.com/download/coil-gun-pdf-free.html>
- [5] D. A. Bresie and J. A. Andrews, "Design of a reluctance accelerator," in *IEEE Transactions on Magnetics*, vol. 27, no. 1, pp. 623-627, Jan. 1991, doi: 10.1109/20.101106.
- [6] B. -S. Go, D. -V. Le, M. -G. Song, M. Park and I. -K. Yu, "Design and Electromagnetic Analysis of an Induction-Type Coilgun System With a Pulse Power Module," in *IEEE Transactions on Plasma Science*, vol. 47, no. 1, pp. 971-976, Jan. 2019, doi: 10.1109/TPS.2018.2874955.
- [7] T. Zhang et al., "Design and Evaluation of the Driving Coil on Induction Coilgun," in *IEEE Transactions on Plasma Science*, vol. 43, no. 5, pp. 1203-1207, May 2015, doi: 10.1109/TPS.2015.2404925
- [8] S.-H. Kim, S.-J. Lee, and J. H. Kim, "Design and experiments of multi-stage coil gun system," *Journal of Vibroengineering*, vol. 18, no. 4, pp. 2053–2060, Jun. 2016, doi: <https://doi.org/10.21595/jve.2016.16615>.
- [9] D. Pivonka, "Three-Stage Coil Gun," Harvey Mudd College, Dec. 2006. Accessed: Apr. 18, 2024. [Online]. Available: <https://pages.hmc.edu/harris/class/e155/projects06>
- [10] N. Nottke and C. Bilby, "A Superconducting Quenchgun for Delivering Lunar Derived Oxygen to Lunar Orbit." National Aeronautics and Space Administration, Austin, Apr. 1990

- [11] J. M. Schroeder, J. H. Gully, and M. D. Driga, "Electromagnetic launchers for space applications," *IEEE Transactions on Magnetics*, vol. 25, no. 1, pp. 504–507, 1989, doi: <https://doi.org/10.1109/20.22590>.
- [12] "Optimization of reluctance accelerator efficiency by an improved discharging circuit," *Science Direct*, 2020. <https://doi.org/10.1016/j.dt.2019.08.013> (accessed Mar. 04, 2024).
- [13] M. U. Manzoor, H. Asif, Shoaib-Ur-Rehman and T. Abbas, "Split coil based design of a coilgun," 2017 13th International Conference on Emerging Technologies (ICET), Islamabad, Pakistan, 2017, pp. 1-6, doi: 10.1109/ICET.2017.8281739.
- [14] N. Ebrahimi, P. Schimpf, and A. Jafari, "Design optimization of a solenoid-based electromagnetic soft actuator with permanent magnet core," *Sensors and Actuators A: Physical*, vol. 284, pp. 276–285, Dec. 2018, doi: <https://doi.org/10.1016/j.sna.2018.10.026>.
- [15] F. Mach, I. Nový, P. Karban and I. Doležel, "Shape optimization of electromagnetic actuators," 2014 ELEKTRO, Rajecké Teplice, Slovakia, 2014, pp. 595-598, doi: 10.1109/ELEKTRO.2014.6848967.
- [16] Masoud Abedinifar, Seniz Ertugrul, and Gokhan Tansel Tayyar, "Design optimization of a solenoid actuator using particle swarm optimization algorithm with multiple objectives," *Advances in Mechanical Engineering*, vol. 14, no. 11, p. 168781322211357-168781322211357, Nov. 2022, doi: <https://doi.org/10.1177/16878132221135737>.
- [17] Sang-Baeck Yoon, Jin Hur, Yon-Do Chun and Dong-Seok Hyun, "Shape optimization of solenoid actuator using the finite element method and numerical optimization technique," in *IEEE Transactions on Magnetics*, vol. 33, no. 5, pp. 4140-4142, Sept. 1997, doi: 10.1109/20.619689.
- [18] "Levi Janssen - YouTube," www.youtube.com. <https://www.youtube.com/@LeviJanssen> (accessed Mar. 30, 2024).
- [18] Queval Loic (2024). Biot Savart magnetic Toolbox
- [19] (<https://github.com/lqueval/BSmag>), GitHub. Retrieved March 31, 2024.
- [20] "capstone/simulator at main · will4269/capstone," *GitHub*. <https://github.com/will4269/capstone/tree/main/simulator> (accessed May 1, 2024).
- [21] "capstone/schematics at main · will4269/capstone," *GitHub*. <https://github.com/will4269/capstone/tree/main/schematics> (accessed May 1, 2024).

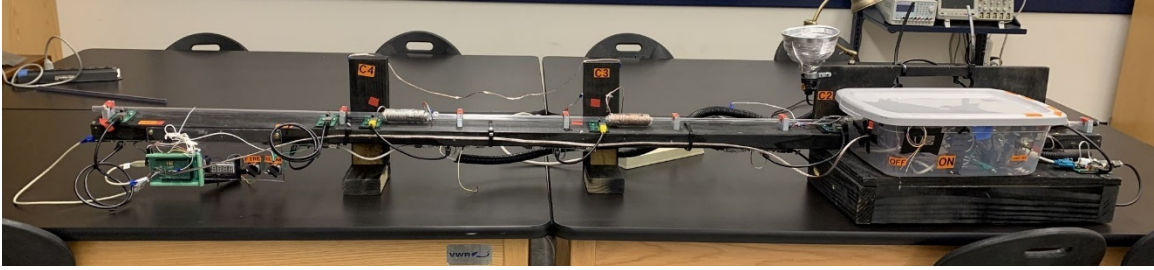
[22] “capstone/data at main · will4269/capstone,” *GitHub*.
<https://github.com/will4269/capstone/tree/main/data> (accessed May 1, 2024).

APPENDICES

Appendix A: Simulator Code

Below is the code exported from MATLAB, with accompanying files [20]. The code was exported to facilitate ease of access and uploaded to GitHub for public access.

Appendix B: System Documentation



System designed and tested, note old test solenoids are on the frame.

Schematics of design documented [21].

MANUFACTURER	PART NUMBER	DESCRIPTION	PRICE	QUANTITY	TOTAL
Vishay	VS-FC420SA10	N-CHAN POWER MOSFET CHASIS MOUNT	\$27.53	6	\$165.18
Vishay	VXA-55-101E	CHASIS MOUNT MOSFETS HEAT SINK	\$4.96	6	\$29.76
South Wire	55797644	250 ft. 16/2 Clear Stranded CU Speaker Wire	\$79.41	1	\$79.41
Essentra Components	145-50M035060K005-ND	HEX SLOTTED SCREW, M3.6 X .6 THR	\$0.60	8	\$4.80
Tecate Group	2085-SCAPPBLS-3.4/27-ND	CAP 3.4F 27V UCAP PACK	\$41.04	4	\$164.16
Vishay	112-VS-40HFR10-ND	DIODE GEN PURP 100V 40A DO203AB	\$5.90	4	\$23.60
Molex	WM7664CT-ND	CONN HEADER SMD 4POS 1.5MM	\$0.70	4	\$2.80
Amphenol Anytek	609-3936-ND	TERM BLK 2P SIDE ENT 5.08MM PCB	\$1.06	10	\$10.60
Bud Industries	377-2624-ND	BREADBOARD GENERAL PURPOSE NPTH	\$4.40	1	\$4.40
Molex	WM1783-ND	MALE MOLEX	\$0.40	10	\$4.00
Molex	WM13070CT-ND	MOLEX MICROFIT CRIMP INSERT	\$0.16	16	\$2.56
Inolux	INL-3ANPT30	THROUGH HOLE / STANDARD 3MM T1 /	\$0.29	25	\$7.33
Lite-On Inc.	LTE-302	EMITTER IR 940NM 50MA RADIAL	\$0.32	25	\$8.08
YAGEO	13-MFR-25FRF52-1KCT-ND	RES 1K OHM 1% 1/4W AXIAL	\$0.06	25	\$1.40
YAGEO	13-MFR-25FRF52-10KCT-ND	RES 10K OHM 1% 1/4W AXIAL	\$0.06	25	\$1.40
YAGEO	13-MFR-25FRF52-34KCT-ND	RES 34K OHM 1% 1/4W AXIAL	\$0.06	25	\$1.40
Würth Elektronik	732-10955-ND	TERM BLK 2POS SIDE ENTRY 5MM PCB	\$0.36	10	\$3.63
Microchip Technology	MCP6566T-E/CTCT-ND	IC COMPARATOR 1 GEN PUR SC70-5	\$0.64	10	\$6.40
Littelfuse Inc.	MCR8SNGOS-ND	SCR 800V 8A TO220AB	\$1.19	10	\$11.92
Molex	WM1813-ND	CONN HEADER R/A 2POS	\$1.18	6	\$7.08
Lite-On Inc.	LTH-301-32	Photo fork	\$1.08	16	\$17.28
Triad Magnetics	237-2008-ND	PWR XFMR LAMINATED 30VA CHAS MT	\$19.06	1	\$19.06
Texas Instruments	256-52996-ND	IC REG LIN POS ADJ 7.5A TO220-5	\$6.25	1	\$6.25
Vishay	KBUSK-E4/51GL-ND	Bridge Rectifier Single Phase Standard 800 V Through Hole KBU	\$4.59	1	\$4.59
Cornell Dublier Electronics (CDE)	338-2273-ND	68000 µF 16 V Aluminum Electrolytic Capacitors Radial, Can - Snap-In 18mOhm @ 120Hz 3000 Hrs @ 85°C	\$6.86	1	\$6.86
Adafruit Industries LLC	1528-1447-ND	Addressable Lighting - 4 Digit LED 7 Segment IFC Blue	\$11.95	1	\$11.95
ARDUINO	A000067	Arduino Mega 2560 Rev3	\$48.40	1	\$48.40
McMASTER-CARR	9176T2	[8ft] High-Pressure Hard Polycarbonate Plastic Tubing for Air and Water, Clear, 3/8" ID, 1/2" OD	\$16.28	1	\$16.28
Chip Quik Inc.	315-NC191LT10-ND	SMOOTH FLOW LOW TEMP SOLDER PAST	\$7.95	2	\$15.90
Techspray	1873-1038-ND	DESOLDER BRAID ROSIN 0.098" 5'	\$4.97	1	\$4.97
Microchip Technology	MCP6561T-E/CTCT-ND	IC COMPARATOR 1 GEN PUR SC70-5	\$0.64	20	\$12.80
Radial Magnets, Inc.	469-1058-ND	MAGNET 0.250"D X 1.000"THICK CYL	\$2.16	2	\$4.32
STMicroelectronics	497-1443-5-ND	IC REG LINEAR 5V 1.5A TO220AB	\$0.65	5	\$3.25
Kobalt	2564346	CRIMP TOOL	\$12.98	1	\$12.98
Gardner Bender	3837165	TERMINATION SET	\$16.48	1	\$16.48
Star Brite	1522051	LIQUID ELECTRICAL TAPE	\$10.98	1	\$10.98
Felit Electric	726998	RED LIGHT BULB	\$4.98	1	\$4.98
Utilitech	203198	CLAMP LIGHT 5.5 INCH	\$9.28	1	\$9.28
JLPCB		PCB 1 order of 5	\$17.63	1	\$17.63
JLPCB		PCB 2 order of 5	\$16.26	1	\$16.26
JLPCB		PCB 3 order of 10	\$22.33	1	\$22.33
JLPCB		PCB 4 order of 10	\$13.42	1	\$13.42
PARTS CABINET		19.9 OHM RESISTOR		1	\$0.00
PARTS CABINET		5K RESISTOR		1	\$0.00
PARTS CABINET		100 OHM RESISTOR		6	\$0.00
PARTS CABINET		470 OHM RESISTOR		6	\$0.00
PARTS CABINET		10K RESISTOR		12	\$0.00
PARTS CABINET		1K RESISTOR		6	\$0.00
STMicroelectronics	497-1443-5-ND	IC linear 5V regulator 1.5A	\$0.65	5	\$3.25
Keystone Electronics	36-7019-ND	female banana connectors - CONN BIND POST DUAL HEX BLK/RED	\$7.95	1	\$7.95
B&K Precision	TL-5A-ND	banana to alligator clips - TEST LEAD BANANA TO GATOR 40"	\$12.00	1	\$12.00
Cai test electronics	CT3089-ND	ADAPT BANANA PLUG TO BANANA JACK	\$7.00	1	\$7.00
Phoenix Contact	277-1796-ND	TERM BLOCK 4POS 45DEG 2.5MM PCB	\$0.67	1	\$0.67
Toshiba Semiconductor	TLP352(F)-ND	OPTOISO 3.75KV 1CH GATE DVR 8DIP	\$1.24	10	\$12.37
Traco Power	1951-1330-ND	AC/DC CONVERTER +/-15V 36W	\$62.91	1	\$62.91
Assmann WSW Components	AE9986-ND	CONN IC DIP SOCKET 8POS TIN	\$0.19	1	\$0.19
SUM					\$942.49

Parts list of design

Appendix C: Plotted Data

Data measured is stored on the MATLAB file [22]. The files were also exported and uploaded to GitHub for ease of public access.

AUTHOR'S BIOGRAPHY

William Poole was born in 2002, and grew up in southern New Hampshire. He was involved in engineering since high school, with electrical an focus prevailing right before college. He attended Pinkerton Academy and was involved with Vex robotics and the swim team. Moving to UMaine in the fall of 2020 he began his major of electrical engineering with a minor in computer science. William is graduating with the degree he signed up for. At UMaine he did not pursue much, he'd rather distract himself for hours working on labs or assignments due weeks later and go out with friends every once in awhile. Will intends to continue to go where his knowledge of electronics and passion for work takes him.